ADVANCED MATERIALS
www.advmat.de

Inter-Aromatic Distances in *Geobacter Sulfurreducens* Pili Relevant to Biofilm Charge Transport

Hengjing Yan, Chern Chuang, Andriy Zhugayevych, Sergei Tretiak, Frederick W. Dahlquist,* and Guillermo C. Bazan**

Biological films containing the microbe *Geobacter sulfurreducens,* as well as protein layers composed of pili filaments, have been recently reported to exhibit electrical conductivities similar to those of doped organic semiconductors.[1,2] The temperature dependence of these conductivities has led to lively debate on the most appropriate transport mechanisms: "electron hopping" or "metallic conduction." One line of thinking proposes that charge equivalents are conducted on pili by a succession of electron transfer reactions among redox proteins.[3,4] An opposing view provides the idea that the pili have metallic conductivity and invokes π–π interchain stacking between aromatic amino acid residues as the critical electron-coupling unit for charge transport.[2,5] Difficulties in purifying pili crystals and identifying the distances between extracellular cytochromes on pili[6,7] prevent the correlation of the electrical properties to an assembled electroactive unit; clear structure-to-property relationships at the molecular level thus remain lacking.

In the area of molecular crystalline organic semiconductors one can find literature precedent of charge-carrier mobilities that can be described by either "band-like"[8,9] or "hopping" transport regimes.[10,11] Heavily doped π-conjugated polymers may also show "metallic" transport with conductivities above 100 S cm^{-1}.[12] In both cases the necessary requirement for sustaining efficient charge transport is the existence of π–π couplings with strength ranging from tens of meV for intermolecular electron transfer, to more than an eV for charge transport along a chain.[13] This need for robust electronic communication between subunits imposes strict requirements on the intermolecular distances and orientations.[14] Pentacene, for example, crystalizes in a layered structure and electronic structure calculations show that both interplanar distances and the tilting of the molecules can affect charge transport depending on the crystal polymorph.[15–17]

Our aim in this contribution is to approach the problem of charge-carrier conduction in *G. sulfurreducens* pili (GS pili) from the perspective of what is known on organic semiconducting materials. We will focus specifically on the conventional charge transport between aromatic units within the protein framework(s). These studies are relevant within the context of ongoing discussions on the extent to which this protein framework is capable of carrier transport in the absence of cytochromes.[3–5] As described in more detail below, we first generated two GS pili subunit (pilin) models by using either homology considerations or nuclear magnetic resonance (NMR) spectroscopy characterization available in the literature.[18,19] These two pilin structures were then used to build corresponding pili models. Inter-aromatic distances and orientations within two pili models were extracted to establish and evaluate electronic π–π couplings between aromatic residues in the pili structure. Finally, electron and hole transfer rates and mobilities within GS pili structure without extracellular redox mediators were calculated based on the small polaron hopping model[13,14] and compared to GS pili experimental data and traditional organic semiconductors.

As shown in **Figure 1**, the GS pilin structure shares considerable sequence similarity to *Neisseria gonorrhoeae* (NG) pilin, the subunit of another type IVa pili.[19] By virtue of this similarity we combined the NG pilin model (**Figure 2**a) and the *G. sulfurreducens* pilin sequence in SWISSMODEL using the automatic modeling mode.[20,21] The resulting homology model ($GS_{Homology}$) of GS pilin, namely the PilA protein, is provided in Figure 2b. We also adopted the existing PilA model of *G. sulfurreducens* pili obtained by solution state NMR spectroscopy[18] to generate GS_{NMR} as shown in Figure 2c. We found both $GS_{Homology}$ and GS_{NMR} models have 40% conserved structure with the NG pilin model and high α-helical contents in N-terminal region (77% for $GS_{Homology}$ and 80% for GS_{NMR}). This high structural conservation of GS pilin with NG pilin led us to hypothesize that their assembly into pili structures would exhibit similar packing.

Based on the molecular 3D coordinates in $GS_{Homology}$ and GS_{NMR}, we extracted inter-aromatic distances by measuring the shortest distance between aromatic ring centers for each pair

Dr. H. Yan
Department of Chemistry and Biochemistry
Center for Polymers and Organic Solids
University of California at Santa Barbara
Santa Barbara, CA 93106, USA
C. Chuang, Dr. A. Zhugayevych, Dr. Sergei Tretiak
Theoretical Division, Los Alamos National Laboratory
Los Alamos, NM 87545, USA
E-mail: serg@lanl.gov
Prof. F. W. Dahlquist
Department of Chemistry and Biochemistry
Department of Molecular
Cellular, and Developmental Biology
University of California at Santa Barbara
Santa Barbara, CA 93106, USA
E-mail: dahlquist@chem.ucsb.edu
Prof. G. C. Bazan
Department of Chemistry and Biochemistry
Department of Materials
Center for Polymers and Organic Solids
University of California at Santa Barbara
Santa Barbara, CA 93106, USA
E-mail: bazan@chem.ucsb.edu

DOI: 10.1002/adma.201404167

Figure 1. Alignment of amino acid sequences from two GS pilin models with the amino acid sequence from *N. gonorrhoeae* pilin (truncated to 70 amino acids). Aromatic residues (red), residues in helical structure (yellow background), and conserved residue (with * and purple background in the bottom row) are highlighted.

of aromatic residues in GS pili (same for subsequent analysis), which are phenylalanine and tyrosine. Inter-aromatic distances within a single pilin monomer exhibit a wide range, from 6.5 to 35.6 Å. These distances, particularly the larger values, are considerably longer than those typical of high mobility organic semiconducting or conducting materials, and immediately argue against a similar transport mechanism. We thus examined other possible contacts as a result of inter-pilin packing in the pili superstructure.

The regions of high sequence conservation between NG and GS pilin are largely responsible for the assembly of the pilus filament in the filament model proposed by the Tainer laboratory from a combination of X-ray and cryoelectron tomography.[19] We thus modeled the assembly in analogy to *N. gonorrhoeae* pili (NG pili), by aligning each GS pilin to NG pilin in PyMol.[19,22] In our approach, the GS pilins were brought together and projected against the previously characterized NG pili structure.[23] As is the case with NG pili, both GS$_{NMR}$ pili and GS$_{Homology}$ pili models exhibit helical arrangements within the GS pili superstructure (**Figure 3**). The diameter of the GS pili in our model ranged from 36.5 to 58 Å, which is consistent with experimental values observed from atomic force microscopy.[2] In the

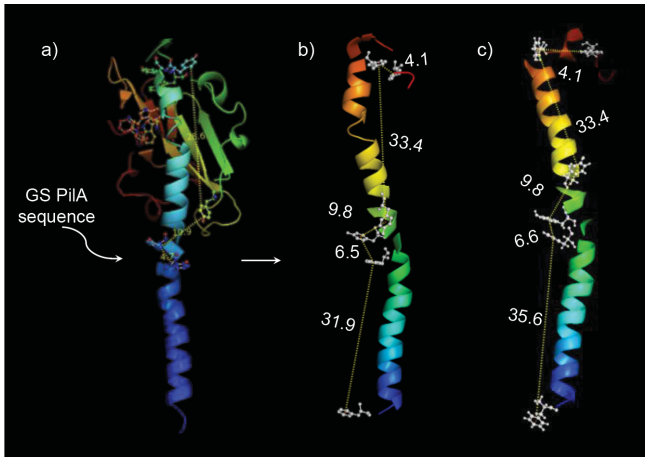

Figure 2. a) *N. gonorrhoeae* pilin model used for building b) *G. sulfurreducens* pilin homology model. c) Another GS pilin model based on NMR spectroscopy results is also adopted in this study. Aromatic residues are shown as stick and ball and the rest are shown in cartoon representation. Inter-aromatic distances (Å) are labeled beside the two GS pilin models.

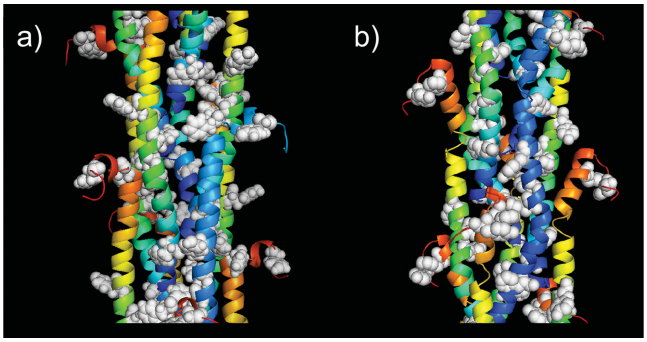

Figure 3. a) The GS$_{NMR}$ pili model built from the GS$_{NMR}$ pilin model and NG pili model. b) The GS$_{Homology}$ pili model built from GS$_{Homology}$ pilin model and NG pili model. Aromatic residues are shown as white spheres and the rest are shown as a rainbow colored cartoon.

GS$_{NMR}$ pili model, phenylalanine-24, tyrosine-27 and phenylalanine-51 are found clustered in the inner space of the pili with inter-aromatic distances of 6.6, 10.4, and 8.6 Å (**Figure 4**). Those three residues from each monomer formed a tentative helical pathway for electron hopping. In the GS$_{Homology}$ pili model, a similar helical pathway of phenylalanine-24 and tyrosine-27 with inter-aromatic distances of 6.5 and 10.8 Å can be identified, see Figure S1, Supporting Information. However, since phenylalanine-51 in both GS$_{Homology}$ and GS$_{NMR}$ pili models is located in the free head C-terminal region, its position is anticipated to be the least accurate due to its higher propensity to perturbations by the environment.

The molecular details of the two pilin models were incorporated into our calculation of electronic structure. A more quantitative evaluation of charge transport properties was accomplished through the application of modeling proven for organic semiconductors. Full technical details of these calculations are given in Supporting Information; we focus here on the principal approach and relevant conclusions. We first computed the electronic properties of the hydrogen-passivated aromatic residues in their actual spatial location. The rest of the protein is modeled as a continuum polarizable medium with the dielectric constant $\varepsilon = 20$.[23] The electronic couplings between the π-conjugated fragments are estimated within the dimer

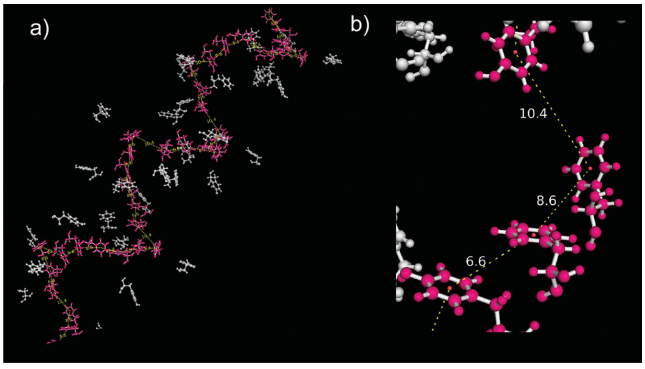

Figure 4. a) Aromatic residues (pink and white stick-and-balls) from GS$_{NMR}$ are extracted. b) Zoomed-in inter-aromatic distances (Å) indicate a helical pathway through identical aromatic residues (in pink) for longitudinal charge transport within pili.

Adv. Mater. **2015**,
DOI: 10.1002/adma.201404167

Table 1. Summary of charge transport properties of $GS_{Homology}$ and GS_{NMR} pili models and experimental values of GS pili and pentacene.

Charge carrier	$GS_{Homology}$		GS_{NMR}		GS pili	Pentacene
	Hole	Electron	Hole	Electron	Exp value	Exp value
Inverse rate [ps]	7.7×10^{14}	1.2×10^{16}	1.1×10^{13}	9.1×10^{12}	N.A.	N.A.
Diffusion coefficient [$cm^2\ s^{-1}$]	1.4×10^{-17}	9.4×10^{-19}	1.0×10^{-15}	1.2×10^{-15}	N.A.	N.A.
Charge mobility [$cm^2\ V^{-1}\ s^{-1}$]	5.6×10^{-16}	3.3×10^{-17}	3.9×10^{-14}	4.7×10^{-14}	N.A.	0.1 to 0.5[b]
Conductivity [$\mu S\ cm^{-1}$]	1.4×10^{-8}		2.0×10^{-6}		6[a]	N.A.

[a]The conductivity of GS pili filament preparation obtained in experiment,[2] where the presence of extracellular cytochromes in the preparation is under debate;[3,4] [b]The charge mobility of pentacene single crystal obtained in experiment.[28]

approximation using density functional theory with CAM-B3LYP functional[24] and 6–31G basis set.[25,26] Thus obtained values do not exceed a few meV, except for isolated pairs. Such minimal interactions suggest the charge-carrier transport regime to be hopping. Inter-fragment transfer rates depend strongly on the reaction transfer energies, $\Delta G°$, which themselves are highly sensitive to the environment. This uncertainty disappears if we are interested only in the upper limit of the transfer rates, which can be reliably estimated by the prefactor of the Marcus formula:[27]

$$w \leq t^2 \sqrt{\frac{\pi}{\hbar^2 \lambda k T}} \tag{1}$$

where t is the electronic coupling and λ is the charge transfer reorganization energy, which is about 0.4 eV for all the residues (intramolecular contribution). For these rates, the dominant charge transfer routes are shown by the inter-aromatic pathways such as that in Figure 4 and Figure S1, Supporting Information. The lowest transfer rates along these routes are on the scale of inverse seconds, dramatically slowing down the electronic transport. As a result, the calculated electron (μ_e) and hole (μ_h) mobilities do not exceed 10^{-14} $cm^2\ V^{-1}\ s^{-1}$ for both $GS_{Homology}$ and GS_{NMR} pili models (**Table 1**), which is at least 13 magnitudes smaller than single crystal pentacene.[28] Under these conditions and by using the relationship between conductivity (σ), mobility, and carrier concentration (ρ), i.e., $\sigma = \rho(\mu_h + \mu_e)$, and using the number density of aromatic residues as the maximum value of ρ leads to σ values of 1.4×10^{-8} $\mu S\ cm^{-1}$ and 2×10^{-6} $\mu S\ cm^{-1}$ for $GS_{Homology}$ and GS_{NMR} pili structures, respectively, compared to the conductivity of GS pili obtained in previous experiment study, i.e., 6 $\mu S\ cm^{-1}$.[2] Even if errors of calculation in conductivities reach to two to three orders of magnitude due to the fluctuations of contact distances in both models (Figure S2 and S3, Supporting Information), they are far below measured values.

We next examine dynamic processes that may impact electronic couplings. Specifically, we used a simplified approach to estimate how the upper limit of conductivity can be influenced by intermolecular (mainly via t) and environmental (mainly via $\Delta G°$) fluctuations.[27,29] Because the charge solvation energy for the aromatic residues (about 2 eV, see Table S2, Supporting Information) is much larger than λ and $\Delta G°$ (tenths of eV), the exponential factor in the Marcus formula is anticipated to fluctuate across a wide range. To remove this uncertainty we replaced it by its maximum value; i.e., unity, as in Equation (1). Fluctuations of intermolecular geometry were modeled by statistical sampling of random translations and rotations with the amplitude matching estimated Debye–Waller factors (DWFs).[30] The upper limit for Equation (1) is given by replacing t^2 by its average value (fast-fluctuations limit).[29] We recognize that the DWF approach may not fully describe bending and/or other temporary deformations within the overall superstructure; however, it is sufficient to explore upper limits of conductivity. The results showed that the deviation of contact distances between the rate-limiting pair fragments for proposed electron transfer in GS_{NMR} (i.e., tyrosine-27 and phenylalanine-51), matching the estimated DWF of about 30 $Å^2$ (Table S11, Supporting Information), will be less than 1 Å (Table S10, Supporting Information). The corresponding transfer integral is on average approximately $10^{-1.5}$ meV, with fluctuations ranging between 10^{-3} and $10^{-1.5}$ meV (Table S10 and Figure S2, Supporting Information). Under these conditions, and assuming the maximum of one charge carrier per aromatic residue, the conductivity can reach up to 100 $\mu S\ cm^{-1}$. Achieving this value requires meeting multiple extraordinary conditions, including the maximum possible values for ρ, which is unphysical, and the exponential factor being unity in the Marcus formula. We can thus conclude that the interaromatic pathway is an unlikely mechanism of conductivity.[14,31]

The work described here provides a perspective of the spatial location of aromatic units within GS pili superstructure based on an analogy to *N. gonorrhoeae* pili, as both share high sequence conservation regions in subunits responsible for superstructure assembly. Moreover, the general approach forms the basis for correlating protein structure with electrical properties. Using the ensemble of aromatic units within the protein as input for quantum mechanical electronic calculation methods leads to charge-carrier mobilities that are insufficient to account for experimentally determined conductivities. The low electronic transport is a consequence that aromatic amino acids are not packed sufficiently tight for π–π interactions. These results based on such a geometry are in contrast with highly cited mechanistic proposals for those biological films,[2,5,6] which invoke inter-aromatic contacts as being critical to the conductivity measurements of biological films, thus paralleling the conductivity mechanisms of biological films with that in conducting conjugated materials. Additional factors that may be relevant to reconcile theoretical analysis and published experimental results include the influence of extracellular cytochromes,[3,4] perturbations by virtue of ion conductivity, differences in pili aromatic content between GS and

N. gonorrhoeae, and protein conformations very far from the equilibrium structures used for calculations here. Despite these uncertainties, the methodology described here provides a potentially general method of correlating protein structure to electronic charge transport.

Supporting Information

Supporting Information is available from the Wiley Online Library or from the author.

Acknowledgements

Funding was provided by the Institute for Collaborative Biotechnologies (ICB) under Grant No. W911F-09-D-0001 from the U.S. Army Research Office. This work was partially supported by LANL LDRD program and the Center for Integrated Nanotechnologies, a U.S. Department of Energy, and the Office of Basic Energy Sciences user facility.

Received: September 9, 2014
Revised: November 17, 2014
Published online:

[1] P. Parisse, M. Passacantando, S. Picozzi, L. Ottaviano, *Org. Electron.* **2006**, *7*, 403.
[2] N. S. Malvankar, M. Vargas, K. P. Nevin, A. E. Franks, C. Leang, B. C. Kim, K. Inoue, T. Mester, S. F. Covalla, J. P. Johnson, V. M. Rotello, M. T. Tuominen, D. R. Lovley, *Nat. Nanotechnol.* **2011**, *6*, 573.
[3] S. M. Strycharz-Glaven, R. M. Snider, A. Guiseppi-Elie, L. M. Tender, *Energy Environ. Sci.* **2011**, *4*, 4366.
[4] S. M. Strycharz-Glaven, L. M. Tender, *Energy Environ. Sci.* **2012**, *5*, 6250.
[5] N. S. Malvankar, M. T. Tuominen, D. R. Lovley, *Energy Environ. Sci.* **2012**, *5*, 6247.
[6] C. Leang, X. L. Qian, T. Mester, D. R. Lovley, *Appl. Environ. Microbiol.* **2010**, *76*, 4080.
[7] T. Mehta, M. V. Coppi, S. E. Childers, D. R. Lovley, *Appl. Environ. Microbiol.* **2005**, *71*, 8634.
[8] O. Ostroverkhova, D. G. Cooke, S. Shcherbyna, R. F. Egerton, F. A. Hegmann, R. R. Tykwinski, J. E. Anthony, *Phys. Rev. B.* **2005**, *71*, 035204.
[9] K. P. Pernstich, B. Rossner, B. Batlogg, *Nat. Mater.* **2008**, *7*, 321.
[10] H. Bassler, *Phys. Status Solidi B* **1993**, *175*, 15.
[11] Y. Olivier, V. Lemaur, J. L. Bredas, J. Cornil, *J. Phys. Chem. A.* **2006**, *110*, 6356.
[12] A. N. Aleshin, *Phys. Solid State* **2010**, *52*, 2307.
[13] A. Zhugayevych, O. Postupna, R. C. Bakus Ii, G. C. Welch, G. C. Bazan, S. Tretiak, *J. Phys. Chem. C.* **2013**, *117*, 4920.
[14] V. Coropceanu, J. Cornil, D. A. da Silva, Y. Olivier, R. Silbey, J. L. Bredas, *Chem. Rev.* **2007**, *107*, 926.
[15] C. C. Mattheus, A. B. Dros, J. Baas, G. T. Oostergetel, A. Meetsma, J. L. de Boer, T. T. M. Palstra, *Synth. Met.* **2003**, *138*, 475.
[16] R. C. Haddon, X. Chi, M. E. Itkis, J. E. Anthony, D. L. Eaton, T. Siegrist, C. C. Mattheus, T. T. M. Palstra, *J. Phys. Chem. B.* **2002**, *106*, 8288.
[17] J. L. Bredas, J. P. Calbert, D. A. da Silva, J. Cornil, *Proc. Natl. Acad. Sci. USA* **2002**, *99*, 5804.
[18] P. N. Reardon, K. T. Mueller, *J. Biol. Chem.* **2013**, *288*, 29260.
[19] L. Craig, N. Volkmann, A. S. Arvai, M. E. Pique, M. Yeager, E. H. Egelman, J. A. Tainer, *Mol. Cell* **2006**, *23*, 651.
[20] K. Arnold, L. Bordoli, J. Kopp, T. Schwede, *Bioinformatics* **2006**, *22*, 195.
[21] L. Bordoli, F. Kiefer, K. Arnold, P. Benkert, J. Battey, T. Schwede, *Nat. Protoc.* **2009**, *4*, 1.
[22] The PyMOL Molecular Graphics System, Version 1.5.0.4 Schrödinger, LLC.
[23] L. Li, C. Li, Z. Zhang, E. Alexov, *J. Chem. Theory Comput.* **2013**, *9*, 2126.
[24] T. Yanai, D. P. Tew, N. C. Handy, *Chem. Phys. Lett.* **2004**, *393*, 51.
[25] R. Ditchfield, W. J. Hehre, J. A. Pople, *J. Chem. Phys.* **1971**, *54*, 724.
[26] W. J. Hehre, R. Ditchfield, J. A. Pople, *J. Chem. Phys.* **1972**, *56*, 2257.
[27] V. Rühle, A. Lukyanov, F. May, M. Schrader, T. Vehoff, J. Kirkpatrick, B. Baumeier, D. Andrienko, *J. Chem. Theory Comput.* **2011**, *7*, 3335.
[28] J. Takeya, C. Goldmann, S. Haas, K. P. Pernstich, B. Ketterer, B. Batlogg, *J. Appl. Phys.* **2003**, *94*, 5800.
[29] D. N. Beratan, S. S. Skourtis, I. A. Balabin, A. Balaeff, S. Keinan, R. Venkatramani, D. Q. Xiao, *Acc. Chem. Res.* **2009**, *42*, 1669.
[30] L. Meinhold, J. C. Smith, *Biophys. J.* **2005**, *88*, 2554.
[31] A. J. Heeger, *Rev. Modern Phys.* **2001**, *73*, 681.

Supporting Information for Modeling inter-aromatic distances in *Geobacter sulfurreducens* pili relevant to biofilm charge transport

Hengjing Yan,[†] Chern Chuang,[‡] Andriy Zhugayevych,[‡] Sergei Tretiak,[*,‡] Frederick W. Dahlquist,[*,†,¶] and Guillermo C. Bazan[*,†,§]

Department of Chemistry and Biochemistry, University of California Santa Barbara, Santa Barbara, CA, USA, Theoretical Division, Los Alamos National Laboratory, Los Alamos, NM, USA, Department of Molecular, Cellular, and Developmental Biology, University of California Santa Barbara, Santa Barbara, CA, USA, and Department of Materials, University of California Santa Barbara, Santa Barbara, CA, USA

E-mail: serg@lanl.gov; dahlquist@chem.ucsb.edu; bazan@chem.ucsb.edu

[*]To whom correspondence should be addressed

[†]Department of Chemistry and Biochemistry, University of California Santa Barbara, Santa Barbara, CA, USA

[‡]Theoretical Division, Los Alamos National Laboratory, Los Alamos, NM, USA

[¶]Department of Molecular, Cellular, and Developmental Biology, University of California Santa Barbara, Santa Barbara, CA, USA

[§]Department of Materials, University of California Santa Barbara, Santa Barbara, CA, USA

Contents

List of Figures

List of Tables

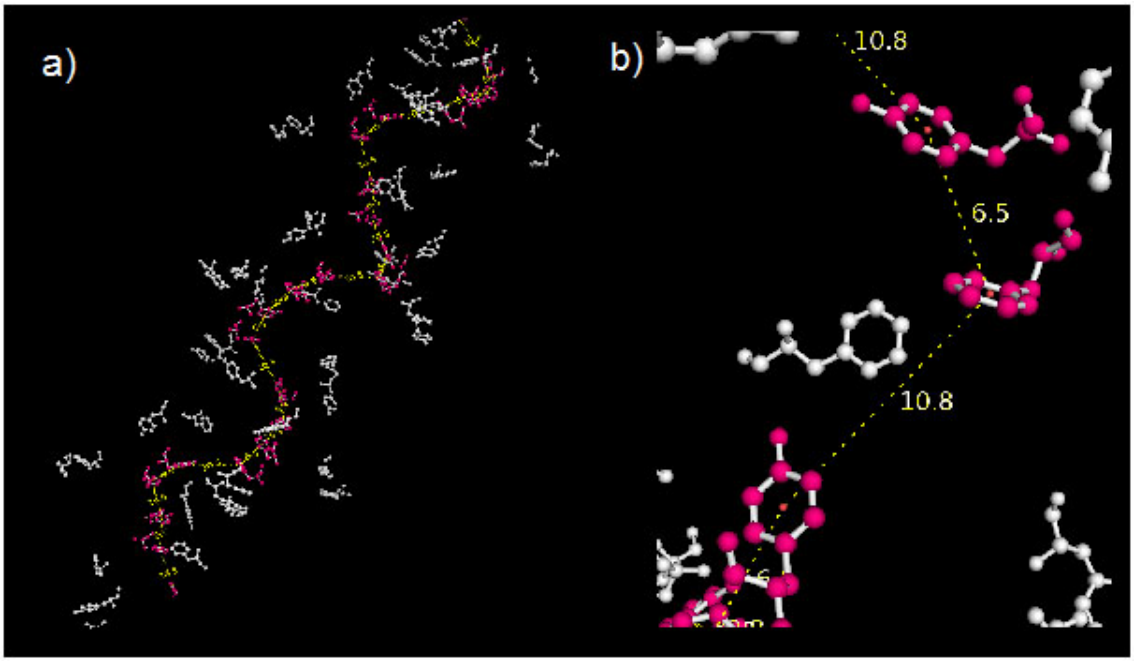

Figure S1: Aromatic residues (both pink and white stick-and-balls) from $GS_{HOMOLOGY}$ are extracted and shown in (a). Zoomed in inter-aromatic distances (Å, yellow dashes and labels) shown in (b) indicate an optimal helix pathway through identical aromatic residues (in pink) for longitudinal charge transport within pili.

S1 Charge Mobilities in Quasi-1D Systems

In accordance to "electron hopping" mechanism, we calculate the charge transfer rates among aromatic residues using the Marcus formula.

$$w = t^2 \sqrt{\frac{\pi}{\hbar^2 \lambda k T}} \exp\left[-\frac{(\lambda + \Delta G^\circ)^2}{4\lambda k T}\right], \tag{S1}$$

where t is the transfer integral, λ is the reorganization energy, and ΔG° is the change in free energy. These are the three key parameters needed to be extracted from quantum chemistry calculations, where we adopt density functional theory (DFT) methodology throughout this study. All calculations are carried out using the Gaussian 09 program[1] with CAM-B3LYP functional[2] and 6-31G basis set[3,4]. The long-range corrected functional CAM-B3LYP provides adequate description of charged states in π-conjugated systems. To facilitate the calculations, we make use of the helical screw symmetry that both $GS_{Homology}$ and GS_{NMR} superstructures possess. We identify the phenylanaline and tyrosine residues that are in close proximity and form a unit cell (Figure 1). In both cases there are six aromatic residues in one unit cell, with the helical screw symmetry parameters $z_0 = 10.5$ Å and $\theta_0 = 100.8^\circ$.

To estimate electrostatic effects of a molecular environment of π-conjugated residues, a polarizable continuum model is employed. Though this model cannot describe a realistic fluctuating local electric fields, it provides the simplest approach for estimating the mean-field magnitude of the effect. The dielectric constant of proteins is not a well defined constant, but its effective local value near residues is large, with the monopole reaction field factor, $(\epsilon - 1)/\epsilon$, close to unity.[5] We set $\epsilon = 20$ following Ref.[5], though any value larger than 10 will have the same rection field factor within 5%. The only essential influence of the polarization effects on the parameters of the charge transport model is in the total energies of the charged residues, see Table S2. Other calculated quantities listed in Tables S1-S5 are not sensitive to changes in dielectric constant.

To characterize the charge carrier mobility of the fully periodic pilin structures, we need

to estimate the Marcus rates among all pairs of the aromatic residues within a unit cell, and those across two adjacent unit cells. These constitute total 30 pairs of residues. The Dijkstra's algorithm[6] is employed to find the dominant charge transfer routes given the rates among the residues. The algorithm gives the shortest path of a directed graph given the distances among the nodes. Here the (directed) distance between a pair of residues is defined to be the inverse of the Marcus rate. The effective rate w_0 given the optimal pathway is defined to be the inverse of the sum of the distances traversing through the path. This rate enters the formula for the diffusion coefficient of the one-dimensional pilin structures as follows

$$D = w_0 z_0^2. \tag{S2}$$

The charge mobility is calculated by the Einstein relation

$$\mu = \frac{eD}{kT}. \tag{S3}$$

To obtain the conductivity of the protein models, we need to estimate the charge carrier concentrations. As an upper bound, we take the number density of the aromatic residues as the density of free holes and electrons in the proteins. Taking the radius of the pilin model to be $r_0 = 35$ Å, the number density of aromatic residues is given by

$$\rho = \frac{6}{\pi r_0^2 \cdot z_0} \approx 1.5 \cdot 10^{-4} \text{ Å}^{-3} = 1.5 \cdot 10^{20} \text{ cm}^{-3}. \tag{S4}$$

Finally, the conductivity is given by

$$\sigma = |e|\rho(\mu_h + \mu_e), \tag{S5}$$

where e is the charge of an electron, and μ_h and μ_e are the mobilities of holes and electrons,

respectively.

S2 Calculations of Marcus Rate Parameters

The *reorganization energy* is defined as follows:

$$\lambda = \lambda^{\mathrm{D}} + \lambda^{\mathrm{A}} = (E^{\mathrm{D}}_{\mathrm{cn}} - E^{\mathrm{D}}_{\mathrm{nn}}) + (E^{\mathrm{A}}_{\mathrm{nc}} - E^{\mathrm{A}}_{\mathrm{cc}}) \tag{S6}$$

where, for example, $E^{\mathrm{D}}_{\mathrm{cn}}$ refers to the energy of the neutral donor residue in the optimized geometry of its charged state (the first subscript refers to the geometry, and the second refers to the charge state). We elaborate the procedures for obtaining the other two parameters as follows: for each pair of residues we calculate the Fock matrix $\mathbf{F}$ and the basis set overlap matrix $\mathbf{S}$ of the total system (dimer) in the ground state. The former can be obtained by the expression $\mathbf{F} = \mathbf{S}\mathbf{T}\epsilon\mathbf{T}^{-1}$, where $\mathbf{T}$ is the eigenvector matrix and ϵ is a diagonal matrix with the eigenvalues as entries. We then define a block diagonal matrix $\mathbf{B} = \mathrm{diag}(\mathbf{T}_1, \mathbf{T}_2)$ composed by the eigenvectors of the two monomers in the ground state (with each MO as a column vector). Subsequently, the projections $\mathbf{F}' = \mathbf{B}^{\mathrm{T}}\mathbf{F}\mathbf{B}$ and $\mathbf{S}' = \mathbf{B}^{\mathrm{T}}\mathbf{S}\mathbf{B}$ are performed. For electron (hole) transport we take out the two-by-two sub-matrices of $\mathbf{F}'$ and $\mathbf{S}'$ corresponding to the LUMO (HOMO) of the two monomers and defined them as $\mathbf{H}$ and $\mathbf{O}$, respectively. The *transfer integral* t is the off-diagonal entry of $\mathbf{O}^{-1/2}\mathbf{H}\mathbf{O}^{-1/2}$, and the *energy offset* is defined by the difference of the two diagonal entries. In Section S3 we set ΔG° equal to the energy offset, while in Section S4 we take into account the effect of environment.

To facilitate the quantum chemical calculations, we further approximate the conjugated residues by their passivated forms. This is done by reserving only the side chains of the residues up to the β carbon atom and replace the chains by hydrogen atoms. More explicitly, a phenylalanine residue is replaced simply by a toluene molecule, and a tyrosine residue by a 4-methylphenol molecule. In this process all of the peptide bondings are removed, even when two conjugated residues are next to each other in the primary structures.

S3 Tables of Charge Transfer Parameters and Rates

Table S1: Reorganization energies of passivated phenylalanine and tyrosine residues in eV.

Charge Carrier	Hole		Electron	
Residue	λ^{D}	λ^{A}	λ^{D}	λ^{A}
Phenylalanine (PHE)	0.17	0.17	0.20	0.22
Tyrosine (TYR)	0.22	0.22	0.22	0.22

Table S2: The energies of the frontier molecular orbitals, the ionization potentials, and the electron affinities in eV. Values in parentheses are the results of vacuum calculations ($\epsilon = 1$).

Residue	HOMO-1	HOMO	LUMO	LUMO+1	IP	EA
PHE	-8.30	-8.00	1.39	1.44	6.58 (8.53)	0.13 (-2.09)
TYR	-8.44	-7.38	1.26	1.71	5.98 (7.87)	0.25 (-1.93)

Table S3: To facilitate discussions, we proxy the relevant aromatic residues by numbers as tabulated here. Since there are six aromatic residues per helical unit cell, residues n and $n + 6$ refer to the same residue in adjacent unit cells.

Residue Number	1	2	3	4	5	6
$\mathrm{GS}_{\mathrm{homology}}$	PHE-24	PHE-51	PHE-1	TYR-27	TYR-57	TYR-32
$\mathrm{GS}_{\mathrm{NMR}}$	PHE-1	PHE-51	PHE-24	TYR-57	TYR-27	TYR-32
	7	8	9	10	11	12

Table S4: Transfer integrals and changes in free energy of $GS_{homology}$ in meV. Only pairs with $|t| \geq 1$ μeV are listed.

Charge Carrier	Hole		Electron	
Residue pair	t	ΔG°	t	ΔG°
2 + 5	-3.6e+01	6.8e+02	-1.1e+02	-1.4e+02
4 + 7	6.5e+00	-7.1e+02	3.3e+00	9.5e+01
6 + 10	-6.4e-05	-1.6e+00	1.6e-03	-5.5e+01

Table S5: Transfer integrals and changes in free energy of GS_{NMR} in meV. Only pairs with $|t| \geq 1$ μeV are listed.

Charge Carrier	Hole		Electron	
Residue pair	t	ΔG°	t	ΔG°
1 + 5	-6.0e-05	6.5e+02	-4.4e-02	-1.1e+02
3 + 5	-2.8e+00	6.5e+02	-5.9e+00	-1.0e+02
3 + 8	-6.2e-02	8.8e-02	9.3e-02	-2.1e-01

Table S6: Inverse Marcus rates of $GS_{homology}$ in ps. Only pairs with $w^{-1} < 1000$ s are listed.

Charge Carrier	Hole		Electron	
Residue pair	Forward	Backward	Forward	Backward
1 + 4	3.8e+26	7.6e+14	1.1e+14	1.2e+16
2 + 5	4.9e+10	2.1e-01	1.7e-02	5.7e+00
4 + 7	1.1e+01	1.1e+13	2.1e+03	4.2e+01
6 + 10	7.1e+11	7.6e+11	4.1e+08	3.3e+09

Table S7: Inverse Marcus rates of GS_{NMR} in ps. Only pairs with $w^{-1} < 1000$ s are listed.

Charge Carrier	Hole		Electron	
Residue pair	Forward	Backward	Forward	Backward
1 + 3	7.6e+12	9.3e+12	6.5e+10	7.3e+10
1 + 5	3.3e+21	4.9e+10	1.9e+05	1.6e+07
2 + 4	1.4e+24	1.9e+13	1.6e+13	5.9e+14
2 + 5	5.5e+23	8.8e+12	1.1e+11	1.1e+13
3 + 5	2.3e+12	2.5e+01	1.1e+01	7.8e+02
3 + 8	2.6e+05	2.6e+05	2.2e+05	2.8e+05
6 + 11	2.0e+14	1.5e+14	2.4e+13	2.6e+13

Table S8: Best charge transport routes in $GS_{homology}$. Values shown in parentheses are the contact distances defined by the closest distance between any two non-hydrogen atoms between the two monomers.

Hole Pathway	Distance (Å)	t (meV)	ΔG° (meV)	λ (meV)	w^{-1} (ps)
$1 \rightarrow 4$	10.8 (8.6)	6.7e-07	7.0e+02	396	7.6e+14
$4 \rightarrow 7$	6.5 (4.6)	6.5e+00	-7.1e+02	394	1.1e+13
Electron Pathway					
$1 \rightarrow 4$	10.8 (8.6)	1.7e-06	-1.1e+02	422	1.2e+16
$4 \rightarrow 7$	6.5 (4.6)	3.3e+00	9.5e+01	446	4.2e+01

Table S9: Best charge transport routes in GS_{NMR}. Values shown in parentheses are the contact distances defined by the closest distance between any two non-hydrogen atoms between the two monomers.

Hole Pathway	Distance (Å)	t (meV)	ΔG° (meV)	λ (meV)	w^{-1} (ps)
$3 \rightarrow 8$	8.6 (5.8)	6.2e-02	8.8e-02	346	2.6e+05
$8 \rightarrow 11$	10.4 (8.4)	4.5e-06	6.4e+02	396	8.5e+12
$11 \rightarrow 9$	6.6 (4.4)	2.8e+00	6.5e+02	394	2.3e+12
Electron Pathway					
$3 \rightarrow 8$	8.6 (5.8)	9.3e-02	-2.1e-01	427	2.8e+05
$8 \rightarrow 11$	10.4 (8.4)	5.5e-05	-1.1e+02	422	9.1e+12
$11 \rightarrow 9$	6.6 (4.4)	5.9e+00	-1.0e+02	441	1.1e+01

S4 Estimations of Environmental Fluctuations and Upper Bounds for Transport

In the natural condition of the proteins of interest, the geometries of the proteins are subjected to constant fluctuations. To take into account the influence from noisy environment and to estimate the upper bounds of the transport properties, we need to investigate how the charge transfer parameters t and ΔG° are affected. As shown in Table S2, the ionization potentials and the electron affinities change by 2 eV upon solvation of the aromatic residues in a dielectric environment of typical biomolecules ($\epsilon > 5$). This means that the amplitude of the fluctuation of ΔG°, caused by fluctuation of local electric field, exceeds λ (Table S1) and energy offset (Fig. S3) substantially. To fully tolerate thus appearing uncertainty in the exponent of the Marcus formula (S1), we use the following expression as the upper limit for charge transfer rate:

$$w \leq t^2 \sqrt{\frac{\pi}{\hbar^2 \lambda k T}}, \tag{S7}$$

where we have simply replaced the exponential factor by its maximum value (the unity). In this expression the only fluctuation-sensitive quantity is t^2. To this end we randomly shift and rotate the relative positions of the two residues in the rate-limiting charge transfer step shown in the previous section (residues 8+11 for electron transfer in $\mathrm{GS_{NMR}}$) and calculate the change in the transfer integral and energy offset. The results are shown in Figures S2 and S3 with details given in Table S10. If we match the amplitude of the fluctuations in our model to the reported Debye–Waller factors for the pilin molecule, $B \sim 20 - 50$, see Table S11 (typical values for proteins[7]), then the corresponding RMS value of the transfer integral t will be in the range $10^{-3} - 10^{-1.5}$ meV. Taking the upper limit and using Eq. (S7) we obtain $w_0^{-1} \sim 100$ ns. Hence $\mu \sim 10^{-5}$ cm^2/V/s and the upper limit for the conductivity is about 0.1 mS/cm.

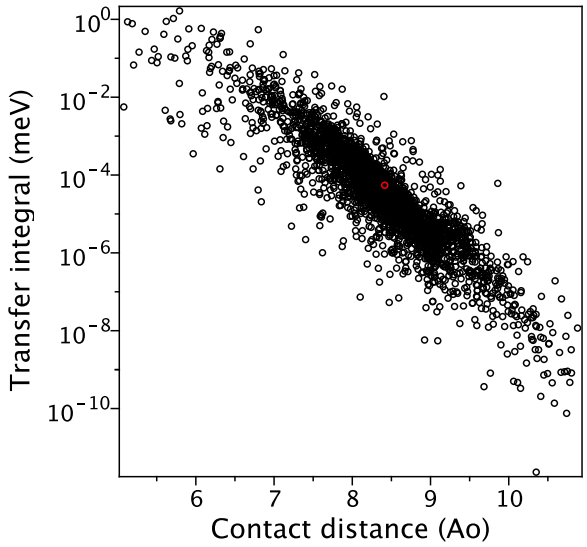

Figure S2: The distribution of transfer integrals in an ensemble of randomized donor-acceptor geometries. The red dot is the original structure given by the residues 8+11 in GS_{NMR}.

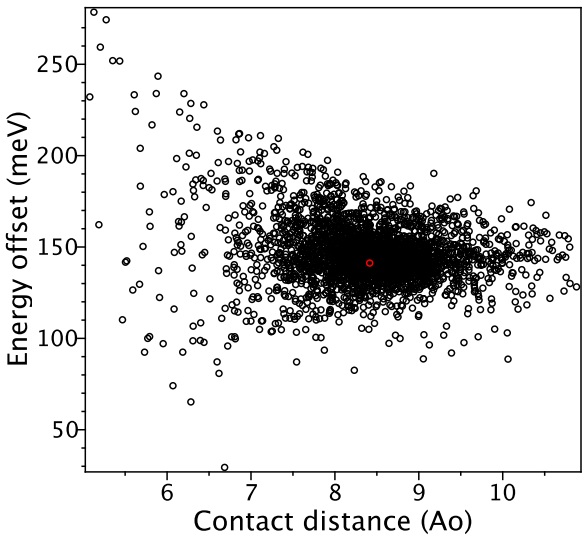

Figure S3: The distribution of the change in free energy in an ensemble of randomized donor-acceptor geometries. The red dot is the original structure given by the residues 8+11 in GS_{NMR}.

Table S10: Details of statistical sampling of fluctuations. Here σ_T and σ_R are the standard deviations for translations (in Å) and rotations (in degrees), respectively. In the Debye–Waller factor, B, hydrogens are not counted. RMS and iRMS correspond to $\langle t^2 \rangle$ and $\langle t^{-2} \rangle$ averages (fast and 1D slow fluctuation limits), respectively.

			cont.dist.(Å)		lg $\lvert t \rvert$ (meV)				ΔG° (meV)	
σ_T	σ_R	B(Å^2)	mean	σ	mean	σ	RMS	iRMS	mean	σ
1/10	10	2.5	8.42	0.20	-4.39	0.42	-4.1	-5.0	-142	5.4
1/4	20	12	8.41	0.46	-4.52	0.87	-3.4	-6.2	-144	11.2
1/3	30	23	8.41	0.63	-4.57	1.11	-2.8	-7.0	-147	14.5
1/2	30	34	8.39	0.81	-4.58	1.45	-1.4	-8.5	-147	15.5
1/2	45	50	8.33	0.89	-4.38	1.54	-1.5	-8.8	-148	20.9
1	90	160	8.38	1.55	-4.66	2.67	0.0	-12.4	-149	32.2

Table S11: Coordinates (in Å) and B-factors (in Å^2) for the rate-limiting pair of fragments in GS_{NMR}.

PHE-51, average $B = 33.4$					TYR-27, average $B = 32.3$				
Atom	x	y	z	B	Atom	x	y	z	B
C_β	8.538	-11.977	-10.971	45.31	C_β	5.409	-8.541	24.722	13.12
C	9.589	-10.898	-10.688	12.34	C	4.657	-7.479	23.892	0.54
C	10.475	-10.488	-11.688	54.42	C	3.374	-7.733	23.393	74.35
C	9.693	-10.291	-9.434	63.50	C	5.239	-6.239	23.585	14.41
C	11.424	-9.512	-11.443	1.22	C	2.698	-6.792	22.636	14.23
C	10.644	-9.315	-9.188	23.23	C	4.565	-5.303	22.827	50.32
C	11.511	-8.927	-10.192	33.45	C	3.297	-5.582	22.352	51.14
					O	2.626	-4.647	21.590	40.10

S5 Derivation of the Debye–Waller factor for our model

In the model considered in the previous section, each fragment is translated by a vector $\vec{t}$, whose components are normally distributed with the dispersion σ_T, and rotated around its geometrical center by a normally distributed angle α with the dispersion σ_R, the rotation axis, $\vec{n}$, is uniformly random on a sphere. Now, for an atom at the position $\vec{r}$ relative to the rotation center, the dispersion of thus randomly shifted position is given by

$$\begin{aligned}\left\langle(\Delta\vec{r})^2\right\rangle = \left\langle\left(\vec{t}+R\vec{r}-\vec{r}\right)^2\right\rangle &= \left\langle\left(\vec{t}\right)^2\right\rangle + \left\langle(\vec{n}\times\vec{r}\,\sin\alpha+\vec{n}\times(\vec{n}\times\vec{r})(1-\cos\alpha))^2\right\rangle \\ &= 3\sigma_T^2 + 2r^2\left\langle\sin^2\theta\right\rangle\left\langle(1-\cos\alpha)^2\right\rangle = 3\sigma_T^2 + \frac{4}{3}r^2\left(1-\mathrm{e}^{-\sigma_R^2/2}\right). \quad \text{(S8)}\end{aligned}$$

The Debye–Waller factor is given by

$$B = \frac{8\pi^2}{3}\left\langle(\Delta\vec{r})^2\right\rangle. \quad \text{(S9)}$$

References

(1) Frisch, M. J. et al. *J. Phys. Chem. B* **1999**, *103*, 252

(2) Yanai, T.; Tew, D.; Handy, N. *Chem. Phys. Lett.* **2004**, *393*, 51

(3) Ditchfield, R.; Hehre, W. J.; Pople, J. A. *J. Chem. Phys.* **1971**, *54*, 724

(4) Hehre, W. J.; Ditchfield, R.; Pople, J. A. *J. Chem. Phys.* **1972**, *56*, 2257

(5) Li, L.; C., L.; Zhang, Z.; Alexov, E. *J. Chem. Theo. Comp.* **2013**, *9*, 2126

(6) Dijkstra, E. W. *Numerische Mathematik* **1959**, *1*, 269

(7) Meinhold, L.; Smith, J. C. *Biophys. J.* **2005**, *88*, 2554